

ZEN2: A narrow J -band search for $z \sim 9$ Ly α emitting galaxies directed towards three lensing clusters.

J. P. Willis^{1*}, F. Courbin², J.-P. Kneib³ and D. Minniti⁴

¹*Department of Physics and Astronomy, University of Victoria, Elliot Building, 3800 Finnerty Road, Victoria, BC, V8P 1A1, Canada.*

²*Laboratoire d'Astrophysique, Ecole Polytechnique Fédérale de Lausanne (EPFL), 1290 Sauverny, Switzerland.*

³*Laboratoire d'Astrophysique de Marseille, Traverse du Siphon BP8, 13376 Marseille Cedex 12, France*

⁴*Department of Astronomy, P. Universidad Católica, Av. Vicuña Mackenna 4860, Casilla 306, Santiago 22, Chile.*

Accepted 2007 September 03. Received 2007 August 24; in original form 2007 July 30.

ABSTRACT

We present the results of a continuing survey to detect Ly α emitting galaxies at redshifts $z \sim 9$: the ZEN (“z equals nine”) survey. We have obtained deep VLT/ISAAC observations in the narrow J -band filter NB119 directed towards three massive lensing clusters: Abell clusters 1689, 1835, and 114. The foreground clusters provide a magnified view of the distant universe and permit a sensitive test for the presence of very high-redshift galaxies. We search for $z \sim 9$ Ly α emitting galaxies displaying a significant narrow-band excess relative to accompanying J -band observations that remain undetected in HST/ACS optical images of each field. No sources consistent with this criterion are detected above the unlensed 90% point-source flux limit of the narrow-band image, $F_{\text{NB}} = 3.7 \times 10^{-18}$ erg s⁻¹ cm⁻². To date, the total coverage of the ZEN survey has sampled a volume at $z \sim 9$ of approximately 1700 co-moving Mpc³ to a Ly α emission luminosity of 10⁴³ erg s⁻¹. We conclude by considering the prospects for detecting $z \sim 9$ Ly α emitting galaxies in light of both observed galaxy properties at $z < 7$ and simulated populations at $z > 7$.

Key words: galaxies: high redshift; clusters; gravitational lensing

1 THE SEARCH FOR THE MOST DISTANT GALAXIES

Observations of distant galaxies provide a direct view of the early stages of galaxy evolution as well as probing the physical conditions of the high-redshift intergalactic medium (IGM). The advent of the Advanced Camera for Surveys (ACS) deployed on the Hubble Space Telescope (HST) in addition to wide field optical cameras operated on 8m class telescopes has provided access to relatively large samples of galaxies located at $z \sim 6$ and beyond. Observations of distant Lyman drop-out galaxies (e.g. Stanway, Bunker & McMahon 2003; Dickinson et al. 2004) and Ly α emitting galaxies selected via narrow-band photometry (Rhoads et al. 2003; Hu et al. 2004) indicate that these bright, distant galaxies cannot be the sole agents of the global re-ionisation demonstrated by studies of Gunn-Peterson absorption in high-redshift quasars (Bunker et al. 2006). Current solutions to this dilemma centre upon the potential contribution of faint galaxies at $z \sim 6$ – pointed to in the very deepest, yet numerically smallest, ACS samples

– or the possibility that an earlier epoch of more intense star formation was responsible for the observed re-ionisation.

Perhaps the most important contribution to the debate concerning the physical nature of bright, high-redshift galaxies has come from Spitzer space telescope observations of rest-frame optical emission in these systems (e.g. Eyles et al. 2005; Yan et al. 2006). Optical to near infrared (NIR) observations of $z \sim 6$ galaxies sample rest-frame emission blueward of the 4000Å discontinuity and are thus sensitive primarily to the spectral contribution from younger stellar populations. The addition of Spitzer/IRAC bands, particularly at 3.6 μ m and 4.5 μ m, samples the potential contribution of older stellar populations in these galaxies. From the limited number of bright $z \sim 6$ galaxies studied to date, there has emerged a picture of their stellar populations as being relatively old (up to 700 Myr) and massive (up to $3 \times 10^{10} M_{\odot}$). The extrapolation of these integrated star formation histories to earlier cosmic times points to an epoch of potentially intense star formation in the predecessors of bright $z \sim 6$ galaxies extending to redshifts $z \sim 10$.

Though compelling evidence points to the existence of actively star forming galaxies at $z > 7$, the direct observation of such sources is far from straightforward – mainly due to the extreme faintness of high-redshift galaxies. The

* E-mail: jwillis@uvic.ca

brightest galaxies observed at $z \sim 6$ display total AB magnitudes of order 24 (e.g. Stanway, Bunker & McMahon 2003; Hu et al. 2004). Galaxies at $z > 7$ – including current samples of candidate systems – can be reasonably expected to display signal levels $AB > 25$ in NIR wavebands (Bouwens et al. 2004). Obtaining a spectroscopic redshift for such faint, continuum selected systems with currently available technology is challenging (though not impossible, c.f. Kneib et al. 2004). Studies employing narrow-band filters or long-slit spectral observations are sensitive to the subset of high-redshift galaxies that emit a significant fraction of their energy in the form of narrow spectral lines – typically the Ly α emission line. Deep narrow-band imaging and subsequent spectroscopic observations have been employed successfully to generate high spectral completeness samples of distant galaxies at redshifts $z = 5.7$ (Hu et al. 2004) and $z = 6.5$ (Taniguchi et al. 2005). Long-slit spectral observations of massive lensing clusters have been employed to investigate the faint end of the Ly α emission luminosity function over the interval $4.5 < z < 5.7$ (Santos et al. 2004) in addition to generating samples of candidate systems in the interval $7 < z < 10$ (Stark et al. 2007). In comparison to narrow-band observations, long slit spectroscopic observations of Ly α emitting sources typically probe a lower background per resolution element yet are normally restricted to relatively small volume studies due to the limited field of view of a spectrograph slit.

A critical unknown factor determining the visibility of the Ly α emission feature in $z > 7$ galaxies is the physical state of the intervening IGM. Absorption studies of $z \sim 6$ quasars appear to have identified the very end of the global re-ionisation process (Fan et al. 2006) while measurement of the optical depth of electron scattering at large angular scales in the CMB points to a typical (though not definitive) epoch of reionisation around $z = 11$ (Page et al. 2006). Clearly then, galaxies at redshifts $7 < z < 11$ may be located in a partly ionised IGM where the local fraction of neutral hydrogen around individual galaxies may be sufficient to attenuate the Ly α emission signature. However, individual Ly α emitting galaxies have been identified in deep, narrow z -band surveys and confirmed spectroscopically at redshifts $z = 6.56$ (Hu et al. 2002) and $z = 6.96$ (Iye et al. 2006). Prompted by such observations, numerous theoretical studies have been undertaken to compute the escape fraction of ultra-violet (UV) photons from a volume of high-redshift intergalactic hydrogen ionised as a result of star formation occurring in an embedded galaxy (Haiman 2002; Santos 2004; Barton et al. 2004). While the detailed properties of the Ly α line transmitted through such a medium are necessarily model dependent, e.g. depending upon the mass, metallicity, star formation rate and initial mass function of the burst and the local density of the IGM, a range of plausible scenarios exist whereby a HII region of sufficient size is created such that transmission of a partially attenuated Ly α line occurs.

The above considerations serve as the motivation for a NIR search for Ly α emitting galaxies at $z > 7$. The search technique employs a narrow J -band filter centred on $1.187\mu\text{m}$ and is sensitive to the signature of Ly α emitting galaxies located at a redshift $z = 8.8$ (termed $z \sim 9$ in the following text). The remaining sections are organised as follows: in Section 2 we describe in further detail the

construction of the narrow-band survey. In Section 3 we describe the techniques used to process the data and identify candidate $z \sim 9$ Ly α emitting galaxies. Finally in Section 4 we determine the co-moving volume at $z \sim 9$ sampled in terms of the Ly α emission luminosity and compare this to a reasonable range of expected properties of $z \sim 9$ galaxies. Throughout this paper, values of $\Omega_{\text{M},0} = 0.3$, $\Omega_{\Lambda,0} = 0.7$ and $H_0 = 70 \text{ kms}^{-1} \text{ Mpc}^{-1}$ are adopted for the present epoch cosmological parameters describing the evolution of a model Friedmann-Robertson-Walker universe. All magnitude information is quoted using AB zero point values.

2 THE ZEN SURVEY

The desirability of detecting very high redshift Ly α emitting galaxies forms the motivation for the “ z equals nine” (ZEN) survey. Ly α emitting galaxies occupying narrow redshift intervals at $z > 7$ will present a characteristic emission excess signature in infrared photometry employing a combination of narrow and broad band filters. Narrow-band, NIR filters tuned to sample regions of night sky emission devoid of strong terrestrial line features provide access to relatively low background signals and thus permit sensitive imaging observations to be executed. In what we refer to as ZEN1 we constructed a 32 hour on-sky image of the Hubble Deep Field South (HDF-S) in the narrow-band filter NB119 employing the VLT/ISAAC facility (Willis & Courbin 2005; WC05 hereafter). Using deep, archival images of the field consisting of VLT/ISAAC J_s -band and HST/WFPC2 optical bands we were able to execute a sensitive test for faint narrow-band excess sources (i.e. $\text{NB} < 25.2$, $J_s - \text{NB} > 0.3$) that remain undetected in optical bands – a practical definition for candidate $z \sim 9$ Ly α emitters. No candidate ZEN sources were identified in these observations. However, the study demonstrated that interloping low redshift emission excess sources could be successfully identified and rejected using deep optical images and that a detailed $z \sim 9$ volume selection function could be computed in terms of Ly α emission luminosity.

As part of a new study – dubbed ZEN2 – we have obtained further narrow and broad band images directed toward the fields of three low redshift galaxy clusters: A1689, A1835 and AC114 (Table 1). Each cluster acts as a gravitational lens and provides a spatially magnified view of the background universe. When considering unresolved sources the effect of this magnification is to increase the total brightness measured within a photometric detection aperture. We therefore use the presence of each cluster along the line of sight to provide a gravitational “boost” to the signal from putative $z \sim 9$ galaxies. The properties of each cluster have been described in detail in the literature and each possesses a well-determined gravitational lens model. Lens models describing the clusters A1689, A1835 and AC114 are presented respectively in Limousin et al. (2007), Smith et al. (2005) and Campusano et al. (2001). Infrared observations of the three clusters were obtained with the VLT/ISAAC facility as part of ESO programmes 070.A-0643, 071.A-0428, 073.A-0475 and are summarised in Table 1. Optical observations of the three clusters consist of HST/ACS F850LP mosaics. These are described briefly in Table 2 and in further detail in Broadhurst et al. (2005) for A1689 and Hempel et al. (2007)

Table 1. NIR data obtained for the three cluster fields.

| Cluster | α (J2000) | δ (J2000) | Redshift | NB119 observations | | | | J -band observations | | | |
|---------|------------------|------------------|----------|--------------------|---------|------|---------------|------------------------|---------|------|---------------|
| | | | | N_{exp} | DIT (s) | NDIT | t_{exp} (s) | N_{exp} | DIT (s) | NDIT | t_{exp} (s) |
| A1689 | 13:11:30.1 | -01:20:17.0 | 0.18 | 54 | 110 | 3 | 17820 | 57 | 35 | 4 | 7980 |
| A1835 | 14:01:02.0 | +02:51:46.7 | 0.25 | 82 | 100 | 3 | 24600 | 40 | 45 | 3 | 5400 |
| AC114 | 22:58:47.7 | -34:48:04.1 | 0.06 | 78 | 100 | 3 | 23400 | 40 | 45 | 3 | 5400 |

Table 2. Properties of the HST/ACS F850LP images of each field.

| Cluster | t_{exp} (s) | Image scale ($''/\text{pix}^{-1}$) | 5σ limiting magnitude within $0''.7$ aperture |
|---------|---------------|--------------------------------------|--|
| A1689 | 28600 | 0.05 | 27.48 |
| A1835 | 18220 | 0.04 | 26.92 |
| AC114 | 18368 | 0.05 | 26.98 |

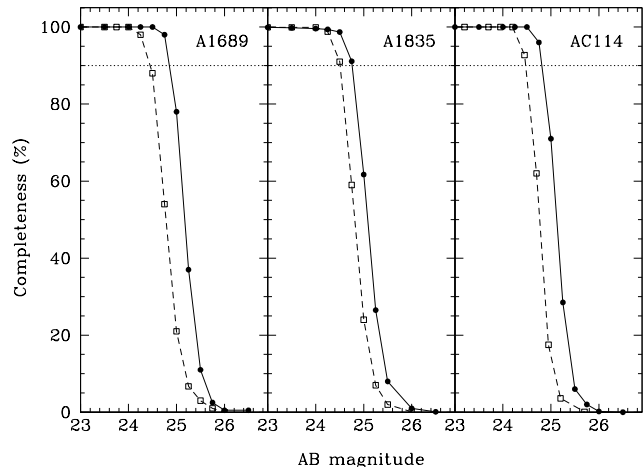
for A1835 and AC114. The NIR observations described in this paper all fall completely within the ACS mosaic areas.

3 DATA REDUCTION AND ANALYSIS

The NIR NB119 and J -band data were processed using techniques essentially identical to those described in WC05 and we summarize them briefly here. Imaging data were a) dark subtracted using standard calibration frames, b) corrected for varying pixel response using twilight sky exposures, c) sky-subtracted having masked array regions containing objects above a specified ADU level, d) corrected for both high- and low-frequency spatial artefacts, and e) shifted to a common pixel scale and coadded using a suitable pixel weighting and rejection algorithm. The image quality in each field and filter combination was computed as the mean full-width at half maximum (FWHM) of a sample of bright, stellar sources visible in each image and is displayed in Table 3.

The J -band observations were obtained under photometric conditions and were placed on an absolute flux scale using observations of standard stars taken with the science data. Reference magnitudes for standard stars observed with the NB119 filter are not available. The NB119 data were therefore placed on an absolute flux scale by comparing the flux measured within a $5''$ diameter circular aperture for a sample of bright, isolated stellar sources visible in both the J -band and NB119 images of each field. The colour term $J - \text{NB}$ for these reference sources is approximately zero and the relationship between J -band reference magnitudes and NB119 instrumental magnitudes is linear and displays a gradient of unity. A total of 12, 16 and 16 such reference sources were employed for the fields A1689, A1835 and AC114 respectively.

Source detection and photometry were performed on each image using the **SEXTRACTOR** software package (Bertin and Arnouts 1996). Once again, we continue the approach outlined in WC05, i.e. source detection is optimised for the detection of marginally resolved or unresolved objects and source fluxes are measured in circular apertures of diameter $0''.7$. The required correction to convert aperture photometry to pseudo-total photometry (assumed to be a $5''$ diameter


Figure 1. Mean detection probability of simulated point sources as a function of AB magnitude within the NB119 (square symbols and dashed line) and J images (circular symbols and solid line). The horizontal dotted line indicates the 90% completeness threshold.

circular aperture) was computed for bright stellar sources in each field. Corrections generated for each image are given in Table 3, though it should be noted that subsequent calculations based upon image photometry all use the $0''.7$ aperture values.

The magnitude corresponding to the 90% point source recovery threshold in each image (m_{90}) was computed by introducing artificial point sources into the reduced image of each field and determining the fraction recovered (see WC05). This procedure produces a low resolution ($3''$ pixels) image of the varying depth of each image. In addition, this process generates a map of photometric uncertainty across each field taking into account contamination by bright galaxies. The average value of the completeness across each image is also displayed in Figure 1 as a function of source magnitude. The magnitudes corresponding to the 90% completeness limit in each field and filter combination are displayed in Table 3. The typical signal-to-noise ratio (SNR) of a source displaying m_{90} in each field is approximately 15. Note that for the purposes of computing the survey selection function in Section 4 we employ the two dimensional completeness information available for each field.

Candidate $z \sim 9$ Ly α emitting galaxies are identified as narrow-band excess sources relative to the J -band reference filter. Figure 2 displays the narrow-band excess versus NB119 magnitude for each of the target fields. We identify emission line sources as those displaying a positive $J - \text{NB}$ signature in excess of the local 3σ uncertainty in $J - \text{NB}$. At the 90% completeness limit of each field this corresponds to

Table 3. Image quality and photometric properties of each reduced image.

| Cluster | Image quality (") | | AB Depth at 90% completeness (0".7 aperture) | | Correction to total magnitudes | | Ly α flux sensitivity ($\times 10^{-18}$ ergs s $^{-1}$ cm $^{-2}$) | |
|---------|-------------------|--------|---|--------|--------------------------------|--------|---|--------------|
| | NB119 | J-band | NB119 | J-band | NB119 | J-band | image plane | source plane |
| A1689 | 0.47 | 0.49 | 24.5 | 24.9 | 0.63 | 0.68 | 3.7 | 0.48 |
| A1835 | 0.42 | 0.42 | 24.5 | 24.8 | 0.56 | 0.55 | 3.6 | 2.38 |
| AC114 | 0.45 | 0.42 | 24.5 | 24.8 | 0.63 | 0.60 | 3.8 | 2.67 |

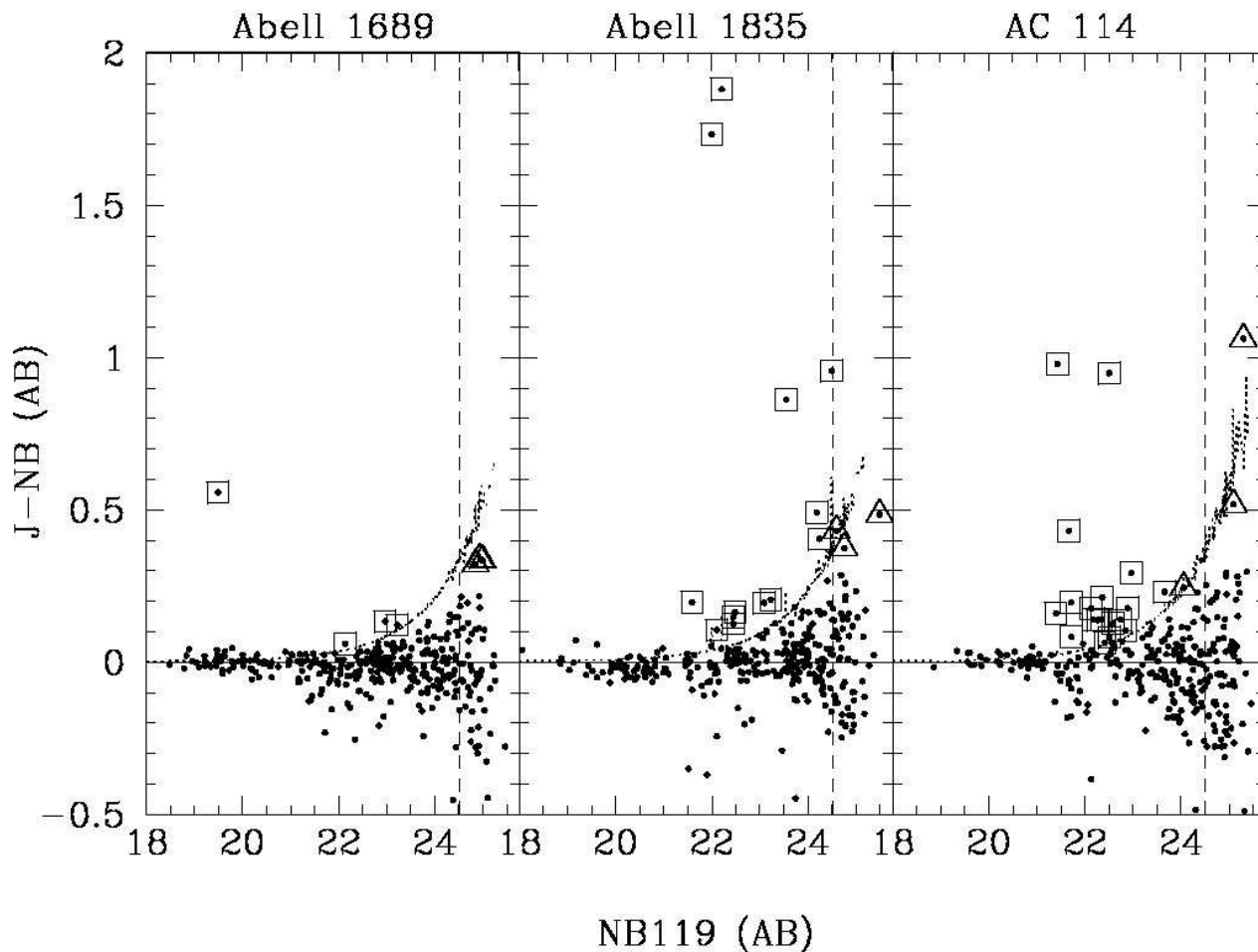


Figure 2. Distribution of narrow-band excess $J - NB$ versus NB119 magnitude for the three cluster fields. Values of $J - NB$ versus NB119 for sources in each field are indicated by dots. For each panel the dotted curve indicates the three sigma uncertainty in the narrow band excess and the solid horizontal line indicates $J - NB = 0$. The vertical dashed line in the each panel indicates the value NB119 $_{90}$. Sources displaying a narrow-band excess greater than the three sigma uncertainty are highlighted using a box. For clarity only sources satisfying NB > 22 or notable brighter sources are marked in this manner. Sources failing the above narrow-band excess measure, yet close to either the selection envelope or the magnitude cut, are indicated with a triangle. These sources were also inspected visually and excluded as potential ZEN sources due to their detection in the corresponding ACS z -band image.

a colour excess $J - NB \geq 0.3$. Of the sources satisfying this narrow-band excess threshold, all are ultimately detected in HST F850LP images of each field. We therefore associate these sources with intervening emission line galaxies (e.g. [OII]3727, $H\beta$ or $H\alpha$) located at redshifts that place the emission feature in the NB119 filter (c.f. WC05). The field of view of the NIR images of each cluster cover an area of 4 square arcminutes in each case. Within this area the images of clusters A1689, A1835 and AC114 respectively contain

4, 13 and 21 interloping emission line sources down to the observed frame magnitude limit m_{90} appropriate for each field. In addition, a small number of sources in each field are detected in the narrow-band but remain undetected in the accompanying J -band. All of these sources were investigated and ultimately associated with faint sources in optical HST observations. Therefore, no candidate $z \sim 9$ Ly α emitting galaxies have been detected in any of the three fields studied.

4 PROBING THE LUMINOSITY FUNCTION OF $z \sim 9$ LAE GALAXIES

The non-detection of candidate $z \sim 9$ Ly α emitting galaxies in the three cluster fields may be understood by computing the total volume sampled at each Ly α luminosity. To achieve this the survey flux sensitivity as a function of solid angle must be corrected for the magnification introduced by the cluster lensing potential in each field, distance dimming and the effect of partial transmission of the Ly α line by the NB119 filter.

The gravitational potential associated with each galaxy cluster creates a magnified view of the background universe. This magnification can be considered as a spatially varying transformation between the source plane and image plane geometry of a particular field. The detection limits displayed in Figure 1 are associated with the image plane of each cluster. The corresponding source plane detection map for each cluster was computed using the LENS`TOOL` package (Kneib 1993) and a model potential describing each cluster. Each pixel in the detection map (location and area) was transformed to the source plane accounting for the varying lens deflection angle as a function of sky position before being re-assembled onto a uniform pixel grid. Images displaying the individual stages in this procedure are displayed in Figure 3.

In Appendix A of WC05 we described how the magnitude limit of a particular narrow-band image could be transformed into a Ly α emission line luminosity at $z \sim 9$ by accounting for the equivalent width criterion applied to select narrow-band excess sources and the partial transmission of the Ly α line by the narrow-band filter. The mean Ly α flux sensitivity toward each cluster field is given in Table 3 and is computed over both image plane and source plane (i.e. de-lensed) pixels. The volume sampled as a function of Ly α luminosity, $V(L_{\text{Ly}\alpha})$, is then computed as the integral over the differential co-moving volume element out to the maximum redshift at which a source displaying the specified luminosity would be detected. We apply the same procedure to determine $V(L_{\text{Ly}\alpha})$ in the current study with only a minor modification: rather than compute the volume sampling based upon the average depth over each field, we compute the volume sampled per pixel in the source plane detection map describing each cluster. The volume sampled as a function of Ly α luminosity for each cluster field is then computed as the contribution from individual detection map pixels, weighted by the solid angle of each pixel. The volume selection function for each cluster is displayed in Figure 4. Each curve is computed assuming a Ly α emission line of rest frame velocity width $\sigma_v = 50 \text{ km s}^{-1}$ (see WC05 for additional details).

The inverse of the volume selection function for the ZEN survey is equal to the cumulative space density of $z \sim 9$ Ly α emitting galaxies sampled as a function of their emission luminosity (Figure 5). The region above each curve in Figure 5 indicates the region of the cumulative luminosity function of putative $z \sim 9$ Ly α emitting galaxies that can be ruled out as a result of the non-detection of bona-fide $z \sim 9$ sources. It is instructive to compare these limits to the cumulative luminosity function both of observed Ly α emitting galaxies at redshift $z = 6.6$ (Kashikawa et al. 2006) and to $z \sim 9$ Ly α emitting galaxies simulated within a semi-

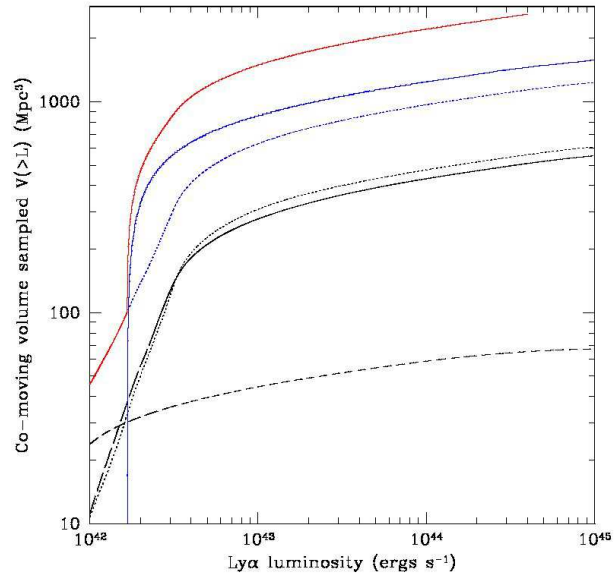


Figure 4. Co-moving volume sampled brighter than a given Ly α luminosity. The black curves indicate the co-moving volume sampled toward each of the three cluster fields in this paper: A1689 (dashed), A1835 (dotted) and AC114 (solid). The blue curves indicate the total co-moving volume sampled toward the three ZEN2 cluster fields (dashed) and the co-moving volume sampled toward the ZEN1 field (HDF-South) described in WC05 (solid). The red curve indicates the total co-moving volume sampled by the ZEN1 and ZEN2 surveys to date.

analytic model of galaxy formation (Le Delliou et al 2006). We consider the implications for each population in turn. If we use the observed population of Ly α emitting galaxies at $z = 6.6$ as a model for emission at $z \sim 9$ then the current areal coverage of the ZEN survey would have to be increased by a factor of at least three in order to provide a realistic constraint on the putative $z \sim 9$ population. The prospect for extending deep, narrow-band surveys at $z \sim 9$ to wider areal coverage is promising given the advent of both the DAZLE (Horton et al. 2004) and HAWK-I (Casali et al. 2006) NIR cameras at the ESO VLT. If instead the properties of Ly α emitting galaxies at $z \sim 9$ are described by the semi-analytic model of Le Delliou et al. then the prospects for their detection is less certain. A small region of the model described by a UV photon escape fraction of 0.2 has already been tentatively ruled out by the ZEN survey. However, reducing the escape fraction to 0.02 results in a proportionate decrease in the Ly α luminosity and the detection of such a population with either DAZLE or HAWK-I will remain challenging. An interesting alternative approach employs the current generation of relatively wide field NIR cameras operating on 4m class telescopes. In Figure 5 we display the anticipated results of ZEN3, a narrow-band search for Ly α emitting galaxies at $z \sim 8$ currently underway using the Canada France Hawaii Telescope (CFHT) WIRC`am` facility (Puget et al. 2004). The exceptional volume sampling of such wide field cameras will permit a very sensitive test of the space density of putative $z \sim 8$ emitters, whether based upon observed $z = 6.6$ or model populations.

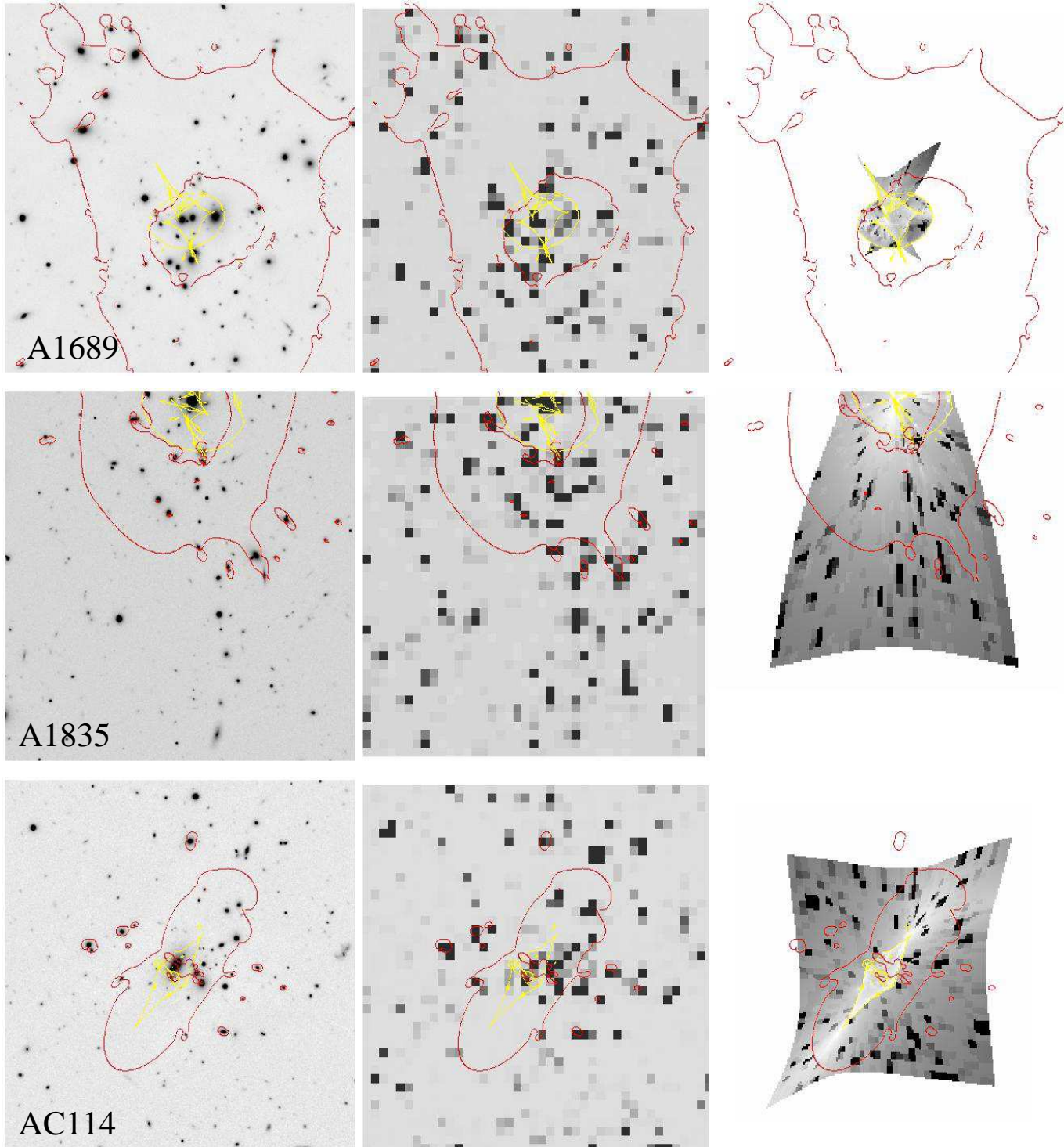


Figure 3. Greyscale images demonstrating the processing applied to the two dimensional sensitivity maps. All images measure two arcminutes on a side with North up and East left. Panels for each cluster are arranged in rows. Left panel: narrow-band image of each field. Centre panel: image plane source detection sensitivity, m_{90} (see text for more details). Lighter regions indicate fainter sensitivity levels. Right panel: Ly α flux detection sensitivity computed for a source plane located at $z = 8.8$. Lighter regions indicate fainter sensitivity levels. The field distortion arises from the inversion of the image plane sensitivity map through the cluster potential. In each panel the red and yellow contours indicate respectively the critical and caustic lines corresponding to a source located at $z = 8.8$.

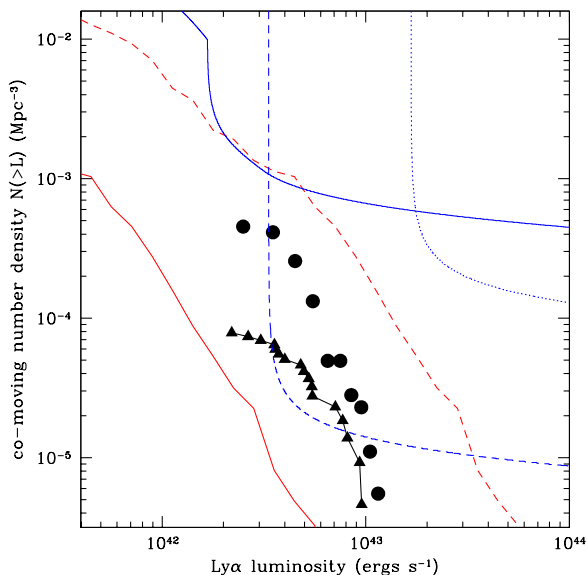


Figure 5. A comparison of the limits imposed upon the $z > 7$ $\text{Ly}\alpha$ luminosity function by existing and planned NIR narrow-band surveys. The blue curves indicate the region of the cumulative space density versus $\text{Ly}\alpha$ luminosity sampled by observations: the ZEN1+2 surveys (solid), the wide area, shallow depth ISAAC survey of Cuby et al. (2006) (dotted) and the planned sensitivity of ZEN3, a wide area NB survey employing CFHT WIRCam (dashed). The points indicate the observations of $z = 6.6$ $\text{Ly}\alpha$ emitting galaxies by Kashikawa et al. (2006): circles indicate the photometric sample corrected for completeness while the triangles indicate the spectroscopically confirmed sample. The red curves indicate the $\text{Ly}\alpha$ luminosity function simulated at $z = 9$ by Le Delliou et al. (2006), assuming a $\text{Ly}\alpha$ escape fraction of 0.02 (solid) and 0.2 (dashed) respectively.

ACKNOWLEDGMENTS

The authors wish to thank both Nobunari Kashikawa and Cedric Lacey for making their data available in electronic form. JPW acknowledges financial support from the Canadian National Science and Engineering Research Council (NSERC). FC acknowledges financial support from the Swiss National Science Foundation (SNSF). DM is partially supported by FONDAP 15010003.

REFERENCES

- Barton, E. J., Davé, R., Smith, J.-D. T., Papovich, C., Hernquist, L., Springel, V., 2004 *ApJL*, 604, 1
- Bertin, E., Arnouts, S., 1996, *A&AS*, 117, 393
- Bouwens, R. J., et al. 2004, *ApJ*, 616, L79
- Broadhurst, T., et al., 2005, *ApJ*, 621, 53
- Bunker, A., Stanway, E., Ellis, R., McMahon, R., Eyles, L., Lacy, M., 2006, *New Astronomy Review*, 50, 94
- Campusano L., E., Pellò, R., Kneib, J.-P., Le Borgne, J.-F., Fort, B., Ellis, R., Mellier, Y., Smail, I., 2001, *A&A*, 378, 394.
- Casali, M., et al. 2006, *Proc. SPIE*, 6269, 29
- Dickinson, M., Stern, D., Giavalisco, M., 2004, *ApJ*, 600, 99
- Eyles, L. P., Bunker, A. J., Stanway, E. R., Lacy, M., Ellis, R. S., & Doherty, M. 2005, *MNRAS*, 364, 443
- Fan, X. et al., 2006, *AJ*, 132, 117
- Gunn, J.E., Peterson, B.A., 1965, *ApJ*, 142, 1633
- Haiman, Z., 2003, *ApJ*, 578, 702
- Hempel, A., et al., 2007 *A&A* submitted.
- Horton, A., Parry, I., Bland-Hawthorn, J., Cianci, S., King, D., McMahon, R., & Medlen, S. 2004, *proc. SPIE*, 5492, 1022
- Hu, E.M., Cowie, L.L., McMahon, R.G., Capak, P., Iwamuro, F., Kneib, J.-P., Maihara, T., Motohara, K., 2002a, *ApJL*, 568, 75
- Hu, E. M., Cowie, L. L., Capak, P., McMahon, R. G., Hayashino, T., Komiyama, Y., 2004, *AJ*, 127, 563
- Iye, M., et al. 2006, *Nature*, 443, 186
- Kashikawa, N., et al. 2006, *ApJ*, 648, 7
- Kneib, J.-P., 1993, Ph.D. Thesis.
- Kneib, J.-P., Ellis, R. S., Santos, M. R., Richard, J., 2004, *ApJ*, 607, 697
- Limousin, M., Richard, J., Jullo, E., 2007, *ApJ* in press (astro-ph/0612165)
- Le Delliou, M., Lacey, C. G., Baugh, C. M., & Morris, S. L. 2006, *MNRAS*, 365, 712
- Page, L., et al., 2006, *ApJ* submitted (astro-ph/0603450)
- Puget, P., et al. 2004, *Proc. SPIE*, 5492, 978
- Rhoads, J. E., et al. 2003, *AJ*, 125, 1006
- Santos, M.R., Ellis, R.S., Kneib, J.-P., Richard, J., Kuijken, K., 2004, *ApJ*, 606, 683
- Santos, M., 2004, *MNRAS*, 349, 1137
- Smith, G.P., Kneib, J.-P., Smail, I., Mazzotta, P., Ebeling, H., Czoske, O., 2005, *MNRAS*, 359, 417
- Stanway, E.R., Bunker, A.J., McMahon, R.G., 2003, *MNRAS*, 342, 439
- Stark, D.P., Ellis, R.S., Richard, J., Kneib, J.-P., Smith, G.P., Santos, M.R., 2007, *ApJ*, 663, 10.
- Taniguchi, Y., et al. 2005, *PASJ*, 57, 165
- Willis, J.P., Courbin, F., 2006, *MNRAS*, 357, 1348
- Yan, H., Dickinson, M., Giavalisco, M., Stern, D., Eisenhardt, P. R. M., & Ferguson, H. C. 2006, *ApJ*, 651, 24

This paper has been typeset from a $\text{T}_{\text{E}}\text{X}/\text{L}^{\text{A}}\text{T}_{\text{E}}\text{X}$ file prepared by the author.